NUMERICAL INVESTIGATION OF BERING SEA DYNAMICS

Jerry Craig Bacon

THESIS

NUMERICAL INVESTIGATION OF
BERING SEA DYNAMICS

by

Jerry Craig Bacon

Thesis Advisor: J. A. Galt

September 1973

Numerical Investigation of

Bering Sea Dynamics

by

Jerry Craig Bacon
Lieutenant Commander, United States Coast Guard
B.S., United States Coast Guard Academy, 1964

Submitted in partial fulfillment of the
requirements for the degree of

MASTER OF SCIENCE IN OCEANOGRAPHY

from the

NAVAL POSTGRADUATE SCHOOL
September 1973

ABSTRACT

Galt's (1972) Arctic numerical model was used to explore the significant dynamics of the Bering Sea. The model was set up and tested for numerical stability. Climatological wind fields were used along with source-sink exchange transports to drive the model. The runs investigated the results of adding or deleting bottom friction, non-linearities and bathymetry. The results obtained by the model were compared to a circulation pattern proposed by Hughes (1972). The model showed that the circulation is strongly bathymetry-dependent and primarily driven by the sources and sinks.

TABLE OF CONTENTS

LIST OF ILLUSTRATIONS

ACKNOWLEDGEMENTS

The author wishes to express his gratitude to those members of the Faculty of the Department of Oceanography who offered assistance in the preparation of this thesis. In particular, he is indebted to Dr. Jerry Galt for his unceasing and timely encouragement throughout the entire study.

He is grateful to Dr. Robert Paquette for his counsel and assistance in putting together this final manuscript. His grateful thanks go to the staff of the W. R. Church Computer Center at the Naval Postgraduate School for their patience and understanding; and to his wife for her faith, encouragement and understanding.

I. INTRODUCTION

The object of this project was to conduct a numerical exploration of large-scale flow of the deep Bering Sea with an initial goal of developing a working numerical model for the desired area. Following this, the most important goal was to study the effects brought about by varying the important oceanographic variables in the model.

The basic model utilized was one developed by Galt (1972, 1973) for use in the Arctic Ocean. This model assumes homogeneous water, has capabilities of varying the depth, and includes lateral and bottom friction. The flow in the model is driven by a wind stress applied at the surface and the introduction of sources and sinks into the vorticity field at the boundaries. This model then was configured for use in the Bering Sea by alteration of the grid field to conform with the study area.

Figure 1 shows the entire Bering Sea basin and shelf area. Two main factors influenced the reasoning used in choosing the deep water basin part of the Bering Sea area for the model. The first was due to a combination of the bathymetry of the Bering Sea and the expected physical limitations of the model. Beyond the northeastern boundary of the model, the Bering Sea bottom is a fairly long, flat continental shelf which presumably will not drastically affect the dynamics of the western portion of the Bering

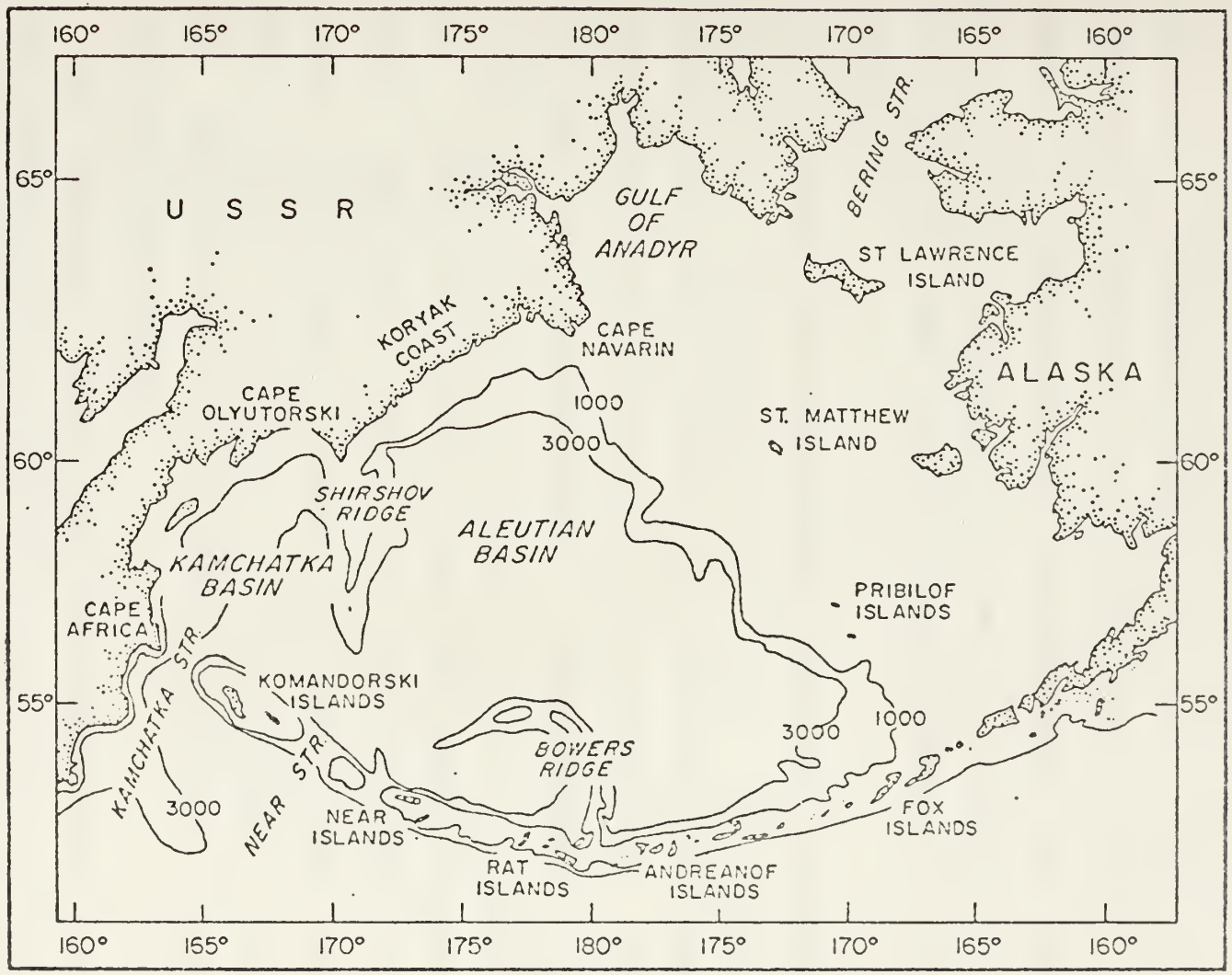

Figure 1. The Bering Sea. Depths in meters.

Sea. Due to the physical configuration of the model area, the mathematical constraints and geometrical limitations placed upon the model [Willems, 1972; Galt, 1973], a larger area was avoided. The second reason deals more with the realities of the basic project. Existing observed and hypothetical data do not extend much further beyond the edge of the continental shelf than the model does and, considering that the model flow was to be compared to this data, the model study area was determined as shown (Figure 2).

The finite grid system used in the model was based on a triangular cell as used by Galt (1972). The resolution of the grid was 1/2° of latitude at 58° North latitude or approximately 30 nautical miles (55.6 kilometers). In the model, the grid was coded as a parallelogram with N columns and M rows, thus giving a total of N x M points (24 x 28 = 672). The grid points were numbered sequentially from left to right by rows. Two additional vector arrays were utilized to specify the extent of the interior domain and are dimensioned M. The area actually studied was coded by use of initial boundary conditions inside the original parallelogram.

As previously stated, one of the primary driving forces for Galt's model is the application of wind on the surface as a stress. The actual wind data utilized for this investigation was obtained from Aagaard [1973]. Source-sink

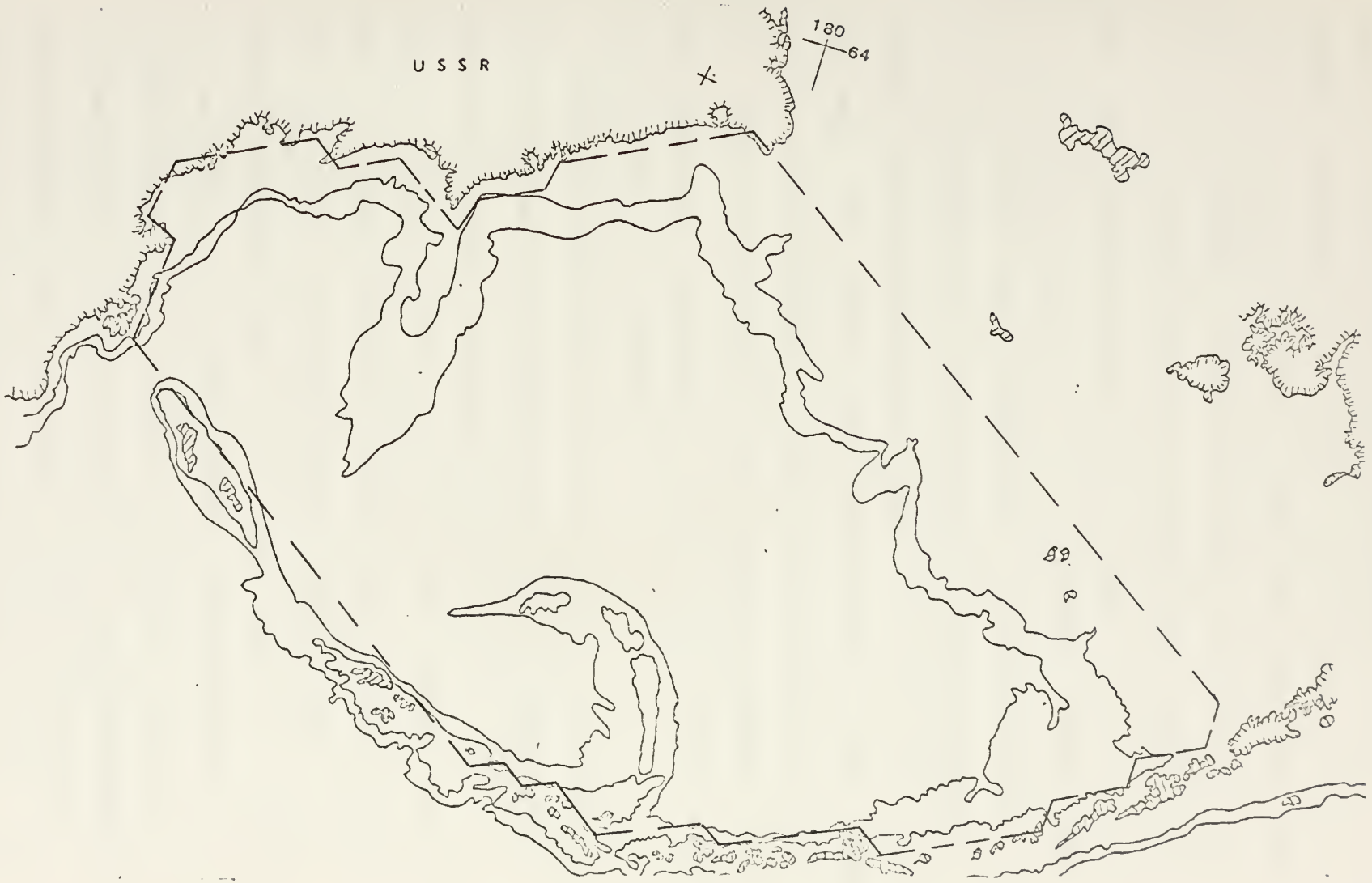

Figure 2. The Bering Sea with model work area delineated. Depth contours at 1000 and 3000 meters.

boundary conditions were taken from Hughes [1972], hereafter referred to as Hughes, and Coachman [1973].

The Bering Sea has been studied for years but, until the work of Hughes, a detailed study of the entire water circulation pattern based on observed data had not been done. One of the results of the several studies conducted is that the wind appears to be the primary driving force for the surface water circulation in the Bering Sea. The real wind fields used for this project were obtained as monthly climatological means taken from atmospheric pressure maps. The obvious point of interest in these fields was the strong increase in force in the winter months. The basic directional driving force, however, remained the same. This maintained a generally cyclonic flow pattern present in the surface circulation.

There had been three basic methods for the determination of circulation in the Bering Sea prior to Hughes' work. The first was the classical dynamical method used for computing geostrophic circulation. This method has never really produced conclusive results due to the scattered and sparse data field available at any one time. The second method has been by water mass analysis. Neither core nor volumetric methods have been used and the isentropic analysis has received little use. The waters of the Bering Sea are characterized by a cold intermediate layer [Hughes] and a similarity to the North Pacific Sub Arctic in the deeper layers [Sverdrup, 1972]. This

then leads to the difficulty in analysis. The third method has been the use of wind-driven models. These have been difficult to establish as a forecasting tool due to the rather inadequate data available and the difficulty in the handling of the averaging methods used on the atmospheric pressure maps [Hughes].

Various Japanese, U.S.S.R., and U.S. investigators have looked at separate sections of the flow pattern in the Bering Sea over the years and, as a result, extensive data files have been gathered by these countries. Hughes combined parts of this data with three years of his own direct observations and measurements, and conducted a thorough study of the single-layer circulation of the Bering Sea deep-water basis. As his measurements were all made during the mid-summer months, Hughes directed his attention mainly to the flow during that period. Based on other data and theoretical work, Hughes does speculate on the flow during the winter months but draws no specific conclusions.

Hughes' work was principally the result of drogue studies and in-situ measurements. Secondarily, Hughes compiled transport flow values through the various straits and around the boundary areas in sufficient detail that a direct application was made to the model where necessary for sources and sinks. To make these calculations, Hughes had to make a rather exact water budget. He obtained

cross-sectional areas of the straits and passes which were considered major inflow and outflow areas. He then calculated water transports and compiled the final budget utilizing the concept of continuity.

Hughes coupled his primary study with a qualitative analysis of bathymetric effects on the circulation. He showed that, due to the Shirshov and Bowers Ridges (Figure 1), the basic cyclonic flow was, in fact, broken into several different gyre patterns surrounding the ridges. Even so, he found that the general overall cyclonic pattern remained.

With Hughes' work as a starting point in the understanding of the flow system in the Bering Sea, the model was then used to explore the significant dynamics in the deep water basin. The results of the model runs were compared with Hughes' work on a qualitative basis only.

There were three fields of variables that required investigation before the model could be run efficiently. Firstly, there were numerical constraints which refer to variable items that control the basic model program and on which final flow pattern results do not depend. Such an item would be the time step used. Secondly, there were configurational constraints, which in this case referred to the geometry of the model. Such items as grid spacing are in this group. The third group consisted of the program parameters. As examples, this list included the variable depths at each grid point, the variable frictional terms, and the variable driving functions.

The variable parameter depth is coded as a depth factor which can be varied to include the entire topographic profile or any percentage thereof, including a flat bottom case or zero percent. This factor alone offered an opportunity to explore Hughes' analysis of bathymetric effects. At the same time as this was being accomplished, the effects of varying lateral and bottom friction and the inclusion and exclusion of non-linearities was explored. Exploratory runs were also conducted to determine the most efficient values of the numerical and configurational constraints to be used.

Sensitivity tests were made on the model to determine its stability with the different parameter field variables working in the model. Throughout these runs, a hypothetical wind force was used as the driving force. Following these runs, a choice was made of the best runs and these were put together with a forcing function derived from climatological wind data to form the final series of runs. These then were compared with Hughes best prognosis of the overall circulation. The next section will deal with the equations used and the actual set up of the model.

II. MATHEMATICS

The area chosen for study includes all of the major topographical features encountered in the Bering Sea; continental shelf, ridges, deep basins, straits, and closed and open boundaries. As has been stated, the major driving forces in the model were wind stress on the surface and a source-sink exchange along the boundaries. Hughes concluded that although the relative magnitudes of the wind stress components were much less in summer than in winter and that even in some cases the wind field became anticyclonic, the overall circulation of the Bering Sea maintained a cyclonic pattern. He also showed that the source-sink transport exchange between the Bering Sea and the Pacific Ocean for the summer months was significant primarily only in the Kamchatka and Near Straits and somewhat in the Buldir Pass. It was suggested that exchanges along the other boundaries were small and of secondary significance in the overall flow scheme for the summer months.

The deep water basin of the Bering Sea is divided by the Shirshov and Bowers Ridges (Figure 1). The depth of water above the ridges is less than 1000 meters and in the basins to either side of the ridges is greater than 3000 meters. Depth within the model was coded as a deviation from the average depth (taken in this case as 3000 meters). All depth values were normalized to this average depth

before entering them in the program. An algorithm was then used that allowed the model to work with percentages of the normalized deviation factors. For example, specifying zero percent resulted in all points having a depth value of one and the model treated the basin as a flat bottom case.

The model used was originally developed as a homogeneous, barotropic model because a baroclinic model would involve much greater complexities in the mathematics than was desired at this stage. In addition, Galt (1972) has shown that there may be depth independent components to the current, and thus, this seemed a useful starting point for a numerical investigation.

The frictional terms of the equations used in the model are of two basic types. One is lateral friction and the other is bottom friction. Although both terms appear in the equation, they are both truly effective only in particular areas. The lateral friction term effects are noticeable along the boundaries when no slip conditions are specified. In a free slip condition there is no boundary for the lateral friction to interact with. Bottom friction is dependent upon and inversely proportional to the depth and basically deals with the dissipation of vorticity. Because of its relation to the depth, it is effective primarily in the relatively shallow areas. It should be noted here that the minimum depth utilized in the model is 0.01 (30 meters) of the normalized averaged depth.

The following development is intended to give the reader a cursory inspection of the basic equations and the methods used to manipulate them. For a more detailed investigation the reader is referred to Galt (1972, 1973). The basic integrated form of the equation of motion was the starting point,

$$\frac{Du}{Dt} - fv = -\frac{1}{\rho}\frac{\partial P}{\partial x} + K\nabla^2 u - \frac{Ru}{h} + \frac{\tau^x}{\rho h} \qquad (1)$$

$$\frac{Dv}{Dt} + fu = -\frac{1}{\rho}\frac{\partial P}{\partial y} + K\nabla^2 v - \frac{Rv}{h} + \frac{\tau^y}{\rho h} \qquad (2)$$

where:

u and v are horizontal components of velocity indendent of depth;

ρ is density and is constant;

τ^x and τ^y are wind stress components;

h is the depth;

f is the coriolis parameter;

both h and f are functions of position;

K and R are constants specifying the effectiveness of horizontal and vertical frictional forces respectively.

Along with these two basic equations of motion, the continuity equation,

$$\frac{\partial}{\partial x}(hu) + \frac{\partial}{\partial y}(hv) = 0 \qquad (3)$$

and the transport stream function equations,

$$-hu = \frac{\partial \psi}{\partial y}\ ,\ -hv = \frac{\partial \psi}{\partial x} \qquad (4)$$

were combined with some manipulation to form the vorticity equation,

$$\frac{\partial \xi}{\partial t} - (\nabla \times \psi \vec{k}) \cdot \nabla \left(\frac{\xi + f}{h} \right) = K \nabla^2 \xi - \frac{R}{h} \xi + \left[\nabla \psi \cdot \nabla \left(\frac{1}{h} \right) \right] + \nabla \times \left(\frac{\vec{\tau}}{\rho h} \right) \tag{5}$$

and

$$\nabla \left(\frac{1}{h} \nabla \psi \right) = \xi \tag{6}$$

where:

$$\xi = \frac{\partial v}{\partial x} - \frac{\partial u}{\partial y}$$

$$\nabla ( ) = \vec{i} \frac{\partial ( )}{\partial x} + \vec{j} \frac{\partial ( )}{\partial y}$$

$$\vec{\tau} = \tau_x \vec{i} + \tau_y \vec{j}$$

With three initial and boundary conditions established in the beginning of the program, the preceding equations were solved for vorticity and stream function. The three conditions which must be specified are:

a) ψ -given within the region of interest at t=0;

b) ψ -given on the boundary of the region for all time, (this one is the same as establishing source-sink boundary conditions);

c) ξ -given within the region of interest at t=0.

After non-dimensionalizing all quantities in the foregoing expressions, an application of the Adams-Bashforth three-level finite differencing scheme was used to integrate the equations. The following non-dimensionalized form of (5) was used: $\frac{\partial \xi'}{\partial t} = g'$

which was integrated with the following scheme:

$$\xi'(t'+\Delta t') = \xi'(t') + \left[\frac{3}{2} g'(t') - \frac{1}{2} g'(t'-\Delta t')\right] \Delta t' \qquad (7)$$

In these last two expressions g' is the finite difference form of:

$$g' = (\nabla \times \psi') \cdot \nabla\left(\frac{a\xi' + f'}{h'}\right) + \beta \nabla^2 \xi' - \frac{\gamma}{h'}\left[\xi' + \nabla\psi' \cdot \nabla\left(\frac{1}{h'}\right)\right] + \nabla \times \left(\frac{\tau'}{h}\right) \qquad (8)$$

The expansion of the terms in (7) contain three non-dimensional coefficients which govern the scaling of the solution and dictate the relative importance of various terms. They are:

$C1 = \frac{\psi}{\nabla^2 DF}$, which governs non-linearities. If C1 = 0, the model considers a linear problem only; α is the Rossby number;

$C2 = \frac{2}{3}\beta = \frac{2K}{3\nabla^2 F}$, controls lateral friction; β is the horizontal Ekman number;

$C3 = \gamma = \frac{R}{DF}$, controls bottom friction; γ is the bottom drag coefficient.

Where:

f is the normalized coriolis parameter utilizing the North pole as a base;

Δ is the finite grid spacing, (55.6 Km.);

D is the average depth of the model;

ψ_o is equal to 1 Sverdrup, (10^6 m^3/sec.).

There is also a fourth term in equation (7) which is of importance. This term represents the torque added per unit

time by the wind stress. This is assumed constant in time and calculated only once at the beginning of the program.

The original integrated Sverdrup transport data used in the actual runs was produced at the University of Washington, by compiling climatological pressure data for a period of six years. This was converted to wind data and finally to wind stress, all done manually (Aagaard 1973). The final form of the data, as it was used, was obtained by integrating in the X-direction from east to west as demonstrated by Sverdrup (1963).

That is:

$$\int M_y \, dx = \int \frac{\text{curl } \tau}{\rho} \, dx \qquad (9)$$

where:

M_y is the mass transport in the Y-direction;

τ is the wind stress;

β is the beta function $= 2\Omega \cos\theta \frac{d\theta}{dy}$;

θ is the latitude;

R is the radius of the earth;

Ω is equal to 2π radians per day.

Differentiating results in an expression for the curl of the wind stress, i.e.,

$$\text{curl } \tau = M_y \cdot \beta \qquad (10)$$

This was the desired input for the model. An algorithm was developed which gave a finite-difference value of the integrated Sverdrup transport program inputs. Multiplying this

by $\frac{\beta}{H(L)}$, where $H(L)$ is the depth at the given point, curl of τ was obtained. The only problem then remaining was the non-dimensionalizing of these terms in order to remain consistent with the remainder of the program. This was done by a multiplication factor of $\frac{\Delta}{F}$.

After integrating the vorticity equation foreward one time-step, an expression relating vorticity and stream function similar to equation (6) was solved by a successive overrelaxation technique as described by Galt (1972). The optimum value of the relaxation variable used in the model was determined from test runs. This configurational constraint is dependent on the grid size and number of grid points, satisfying the expectation that the relaxation is a function of the geometry of the model.

Prior to executing the series of runs to describe the barotropic flow driven by the realistic wind data, it was necessary to run a series of exploratory tests on the numerical and configurational constraints and the parameter field. The following section will deal with these exploratory runs and the sensitivity and stability tests made on the model.

III. EXPLORATION

Once the model was put together in a running mode, a series of test runs were made in order to determine appropriate values for model variables and parameters. The first investigated was the relaxation constraint. Initially runs were made varying the relaxation value from 1.20 to 2.00. A plot of the relaxation constraint versus number of iterations per time step was made. A value of 1.80 was determined to maximize the convergence rate for the given model geometry.

A value, empirically determined from Arctic model tests (Galt 1973) was initially used for C2, the controlling parameter for lateral friction terms in the equations just discussed. This value was derived utilizing a K value of 10^8 (in non-dimensional units), which is consistent with the lateral friction used in other model studies. Throughout the test runs and later during the actual runs the value was varied periodically to check the model's sensitivity to this parameter. The different values used were on the order of one magnitude either side of the original derived value for C2. In all cases the model results, using these different values of C2, were interpreted as having less realistic energy buildup. Thus, the original value determined was used for all further runs.

The time step value was investigated next. An original

value of 0.5 was chosen as a normalized value corresponding to a half pendulum day. Since F was scaled on the polar value (latitude = 90°), this was equivalent to taking a time step of twelve hours. Runs were made varying this numerical constraint to see what dependence, if any, there was on the numerical stability of the model. When running with the full bathymetry factor in the model, non-linearities and bottom friction terms set to zero, and using a constant torque applied as a driving force, the model achieved steady state solutions only with a time step of 0.0125 or less. With time-step values above this, including 0.5, numerical instability resulted. However, once the bathymetry factor was lowered from 1.0 or 100%, the original value of 0.5 gave satisfactory results in all cases tested. The value of 0.5 was chosen then as the standard time step to use throughout the model.

Due to the irregularities noted in stability at a depth factor of 1.0 in the last test series, the next examination was conducted to determine the model dependency on the bathymetry. In Galt's (1972) original work, the flow in the Arctic model was relatively sensitive to bathymetry, particularly in the area of ridges. Hughes also showed qualitatively that the flow of the Bering Sea is affected by topographic relief on the ocean bottom. The kinetic energy, as an output value in the program, was determined by summing the kinetic energy calculated at each grid point. It was considered to be a good value to monitor for detecting

stability or instability. In all cases, total kinetic energy was therefore monitored and proved to be a sensitive indicator of stability and displayed a dependence on bathymetric modifications. Based on Hughes' work, it was expected that there would be a bathymetric dependency on the flow of the Bering Sea. It was expected that steady state conditions would be achieved under approximately the same conditions as in the Arctic.

The first plot of kinetic energy versus bathymetry percentage was made on the model with C1 (non-linearities) and C3 (bottom friction) equal to zero and a constant torque driving the flow. In all runs where constant torque was applied, a force per unit area approximately 2.9 dynes was applied across the entire basin area. No source-sink conditions were applied in these cases. The same runs were then redone with source-sink conditions applied along the western boundary of the study area, specifically in the Kamchatka, Near and Buldir Pass Straits. From Hughes' work, the source-sink values applied were specified as follows (Figure 3): 25×10^6 m^3/sec. outflow through the Kamchatka Straits; 5×10^6 m^3/sec. inflow between the Komandorski Islands; 5×10^6 m^3/sec. outflow in the western section of the Near Straits; 30×10^6 m^3/sec. inflow spread over the eastern portion of the Near Straits; and 5×10^6 m^3/sec. outflow through the Buldir Pass. Figure 4 shows results of these runs. It should be noted that the best curve fit to the data is approximately exponential.

Figure 3. Transport values used as western boundary source-sink initial conditions. (10^6 m^3/sec.)

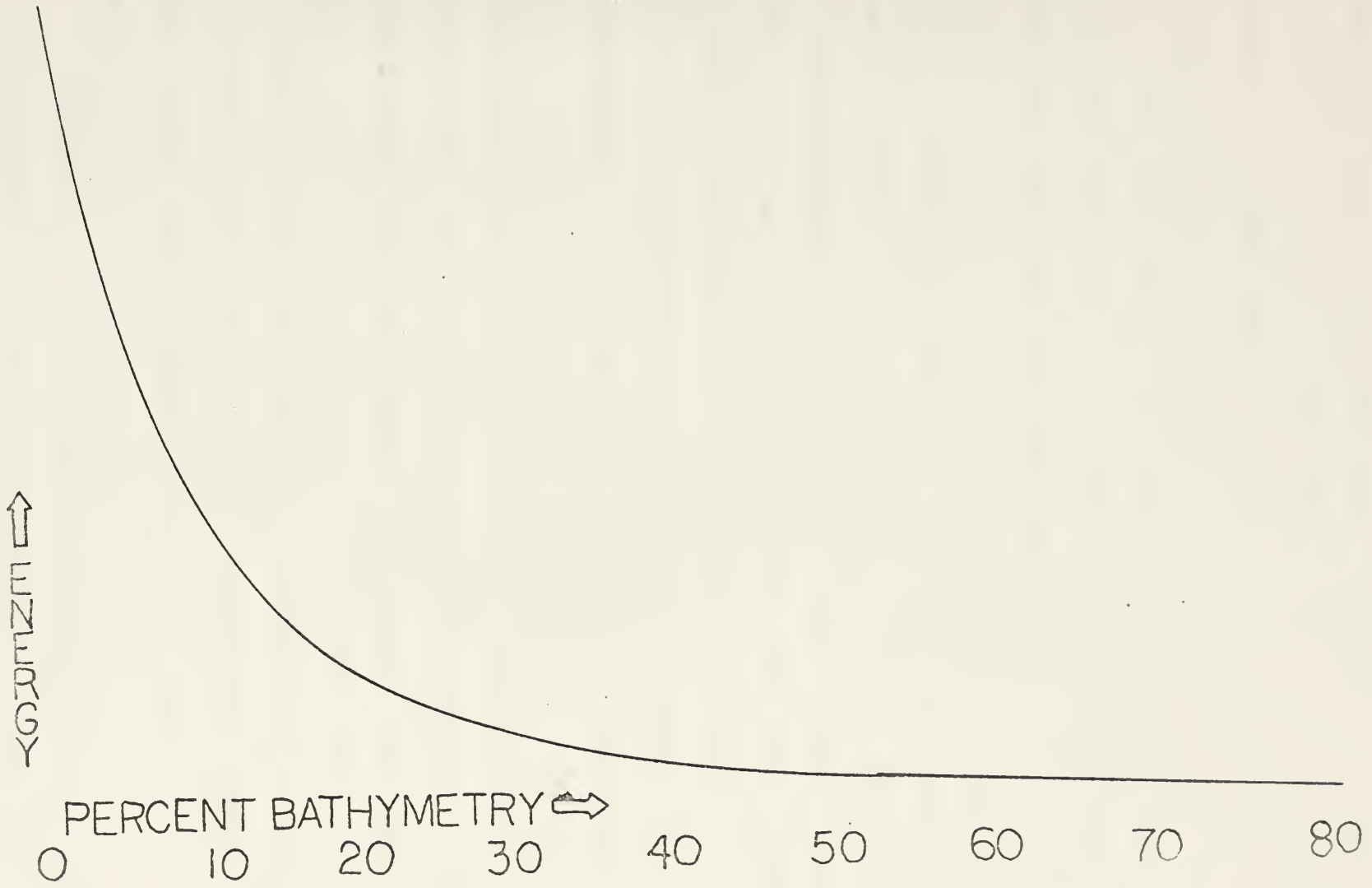

Figure 4. Energy versus bathymetry for cases with constant wind and lateral friction only.

A determination was made on the basis of these plots that runs utilizing 20% bathymetry would satisfactorily describe the relevant dynamics. As a check on this decision, some duplicate runs were made at 50% bathymetry later on and no appreciable qualitative difference in the flow was noted.

Plots were then made of kinetic energy versus normalized time steps of the same set of runs. Initially all runs were terminated after 600 time steps, regardless of flow conditions. At that stage, the program produces a data file which is stored for future use. This data file contains the existing run parameters at time step 600 so that runs may be started at that point and continued further in time. These plots were then extended to 1800 time steps (Figure 5). A stability determination was made from this type of plot. A run that showed energy build-ups leveling off and reaching or, at least, definitely approaching asymptotically a steady state condition with increasing time was considered to be stable. Most runs were approaching steady state conditions at 600 time steps except the flat bottom cases which were running out to almost 1800 time steps before settling down into steady state conditions. It should be noted that running the model as a flat bottom basin under these conditions was simulating the dynamics of Munk's model (1963). Therefore the results were somewhat anticipated for these runs.

The next set of runs were made with only source-sink driving conditions on the western boundary. These runs

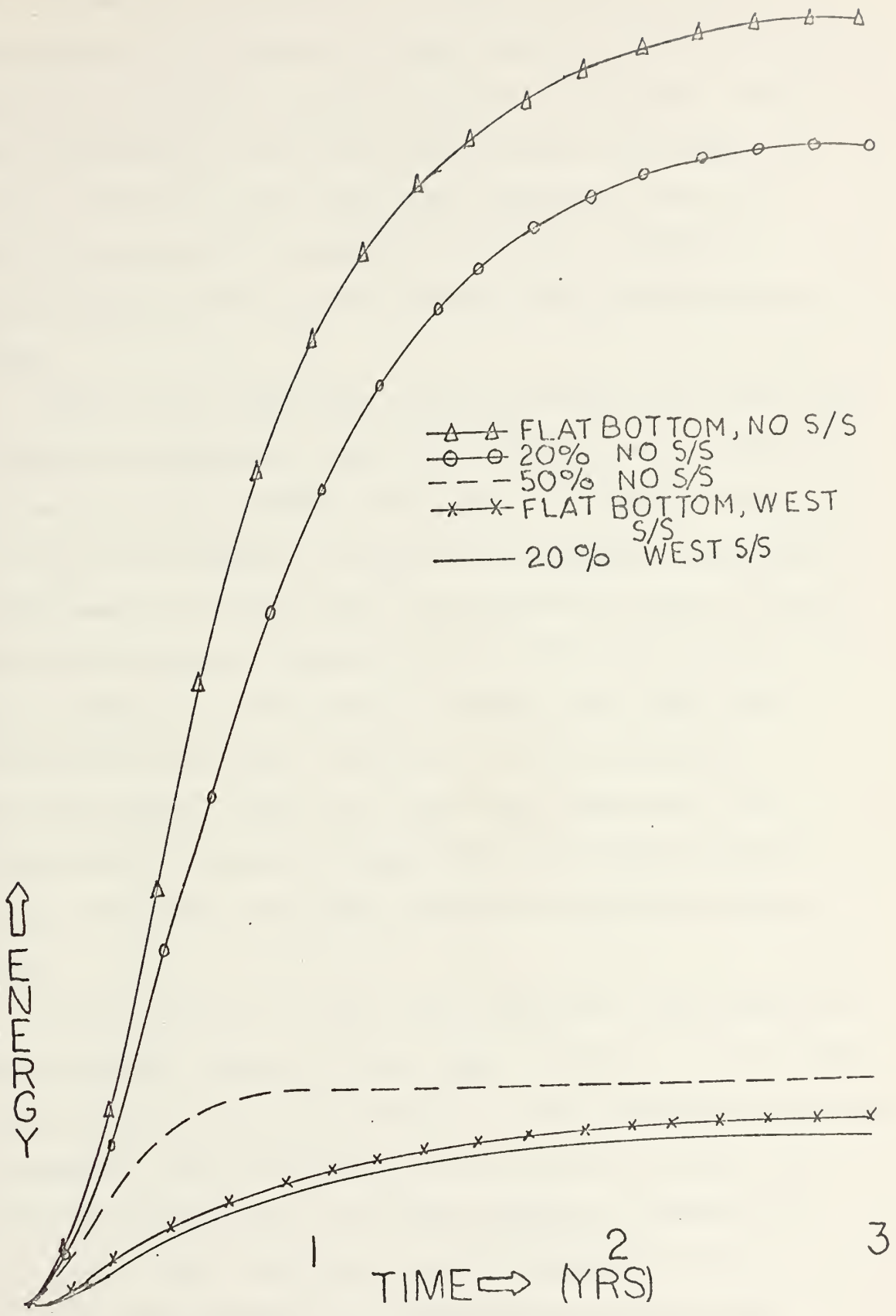

Figure 5. Kinetic energy versus time.

were intended to determine two items. The first was a comparison of the pattern of the resultant flow to that caused by a constant torque driving force. These results were compared for the flat bottom and the 20% bathymetry cases. Secondly, these runs were designed to test the model once again for stability but using a different forcing function in the flat bottom, 20% and 50% bathymetry cases.

Under these conditions, there appeared to be much less bathymetric dependence among the different runs. The first run was with flat-bottom conditions. As would be expected, with the 50% bathymetry example, the transient topographic Rossby waves (Veronis 1966) had relatively high velocities and the circulation pattern settled down very quickly, in approximately 200 time steps. However, all cases had reached a steady-state condition by 600 time steps. With the present conditions, the model appeared to be sufficiently sensitive to numerical and configurational constraints while remaining stable throughout the timed runs.

Before going on to the runs using the climatological data with the addition of the other variables, it was felt necessary to make further checks on the circulation patterns developed. This was done to check consistency with the expected results due to the known dynamics involved to this point. The first case run was conducted with a constant torque applied as the driving function with

no sources and sinks added. Non-linearities and bottom friction were left out (C1 = C3 = 0). The run started with the water initially at rest. A constant depth condition was imposed while the coriolis parameter varied with latitude. Under these conditions, a strong gyre within the basin was expected with some intensification in the western portion similar to Munk's model (1963). Figure 6 shows that this was basically what was achieved. The steady state condition of this flow represents a balance between the torque applied by the wind and the dissipation of same by the lateral friction working on the model.

The second case to consider is the same as the first with the exception that 20% of the bathymetric deviations from the mean depth were allowed to interact. In this case, it was expected that the flow pattern would still basically be cyclonic although now, topographic Rossby waves were possible (Veronis 1966). Under these conditions, the flow could be expected to be broken into sub gyres centered in the basins around the Shirshov and Bowers Ridges. The results showed all this (Figure 7). During the spin-up, propogation of a Rossby wave was noticed moving across the study area from east to west. Cross ridge flow was observed in this case.

The third case involved increasing the bathymetry to 50%. As expected, this did not change the pattern drastically. However, the spin-up time to reach steady state conditions was reduced as could be anticipated and less transport was noticed.

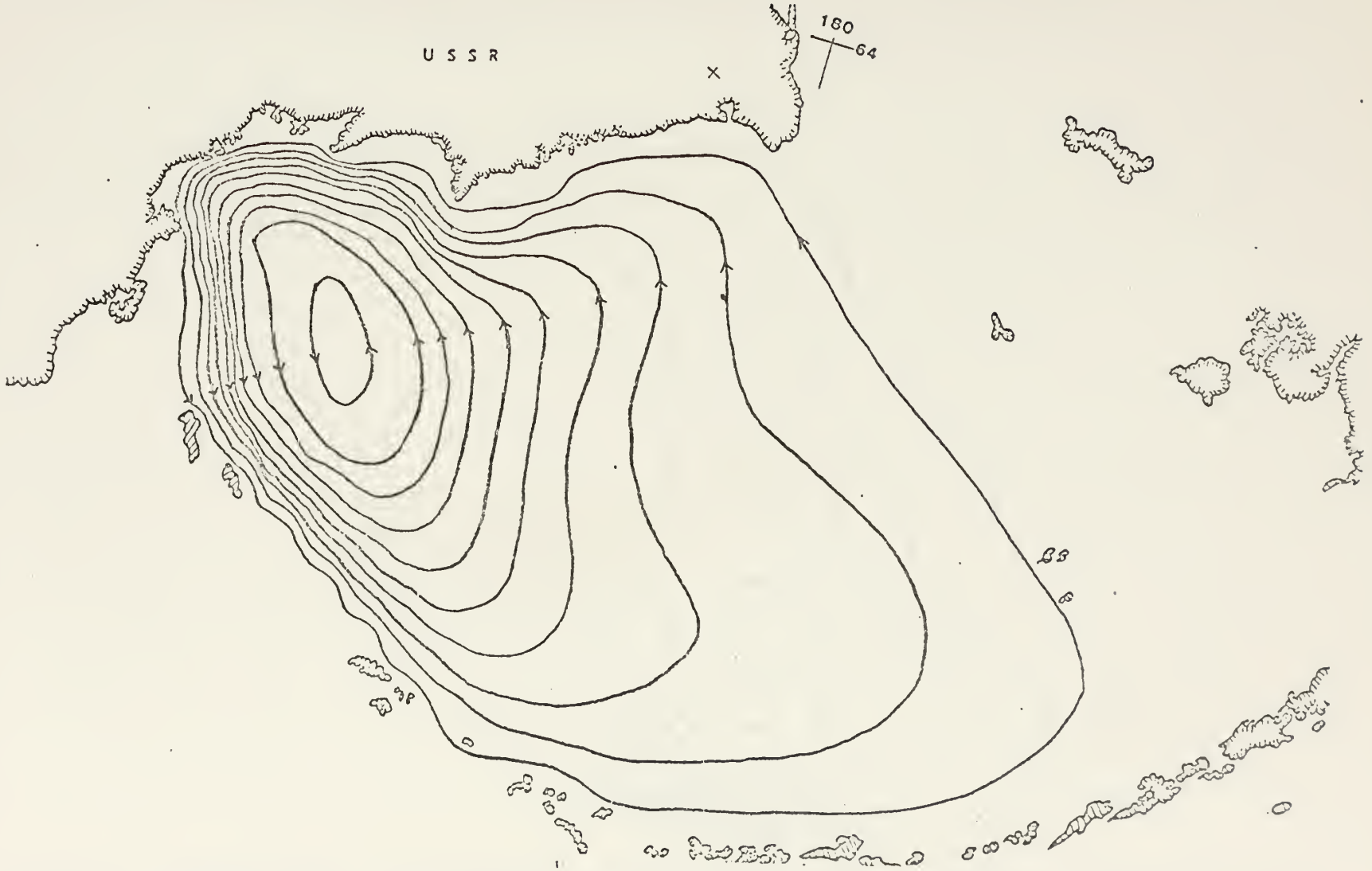

Figure 6. Constant wind, no source-sinks, flat bottom, and lateral friction. Transports in 5×10^6 m^3/sec.

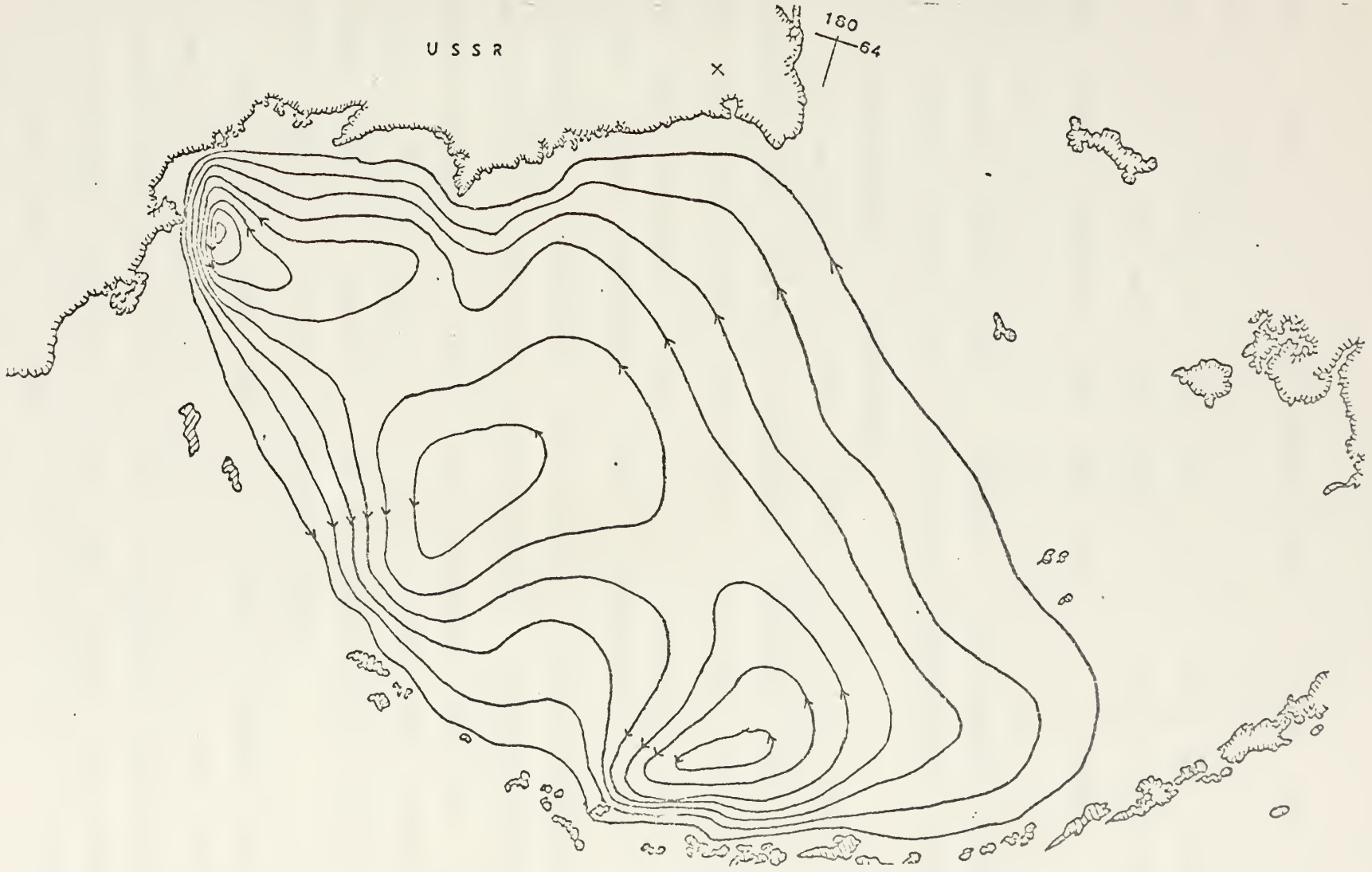

Figure 7. Constant wind, no source-sinks, 20% bathymetry, and lateral friction. Transport interval is 2 x 10^6 m^3/sec.

The next series used sources and sinks on the western boundary as forcing functions. The wind torque was taken as zero. Again, non-linearities and bottom friction were excluded. The first case looked at a flat bottom situation. The flow was driven by the input-output, source-sink initial conditions. Two small gyre patterns were established along the western boundary of the area (Figure 8). The gyre patterns along the boundary were a result of the localized source-sink driving force. The gyre in the northwest corner was a result of the effects of the driving function combined with the geometry of the model.

The second case of this series looked at the basic situation with 20% of the bathymetry included (Figure 9). The gyres created were the same as in the flat bottom case, with some noticeable effect from the bathymetry. The obvious effects of the bathymetry involve the magnitude of the transports. As expected, the transport volumes within the major portion of the basin were reduced. The large-scale anticyclonic gyre around the major portion of the area was a result of the bathymetry forcing the basic flow across the ridges along the boundary. The small gyre in the south is being contained there by the Bowers Ridge.

In comparing the effect of wind and of sources and sinks separately at this point, it appeared that the major driving force for the model was the wind as opposed to the sources and sinks which appeared to have large effects only within their localized area. Both of these series were now rerun

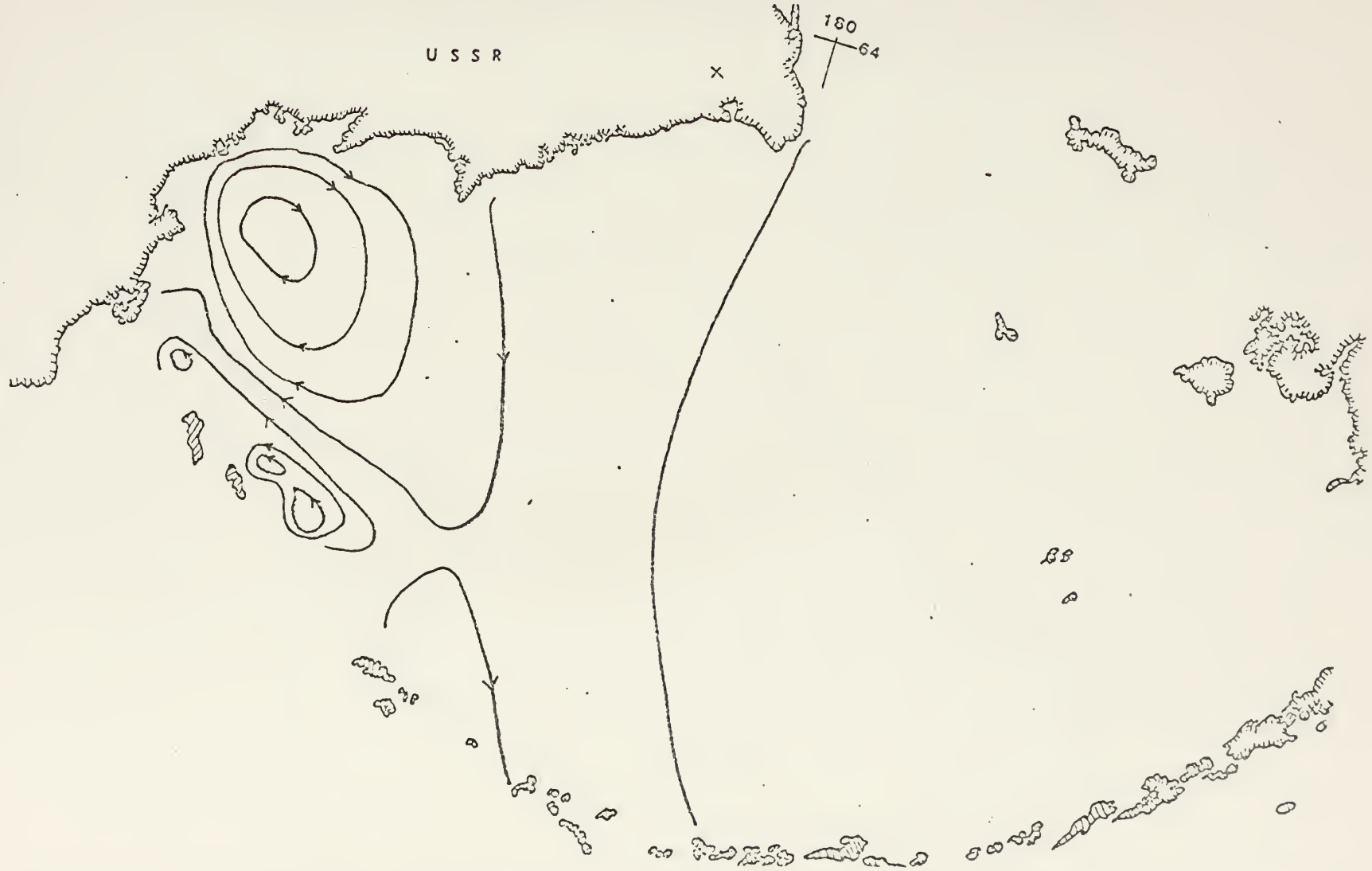

Figure 8. Western boundary source-sinks, no wind, flat bottom, lateral friction. Transport interval: 5 x 10^6 m^3/sec. in anticyclonic gyre; 10 x 10^6 m^3/sec. in cyclonic gyre.

Figure 9. Western boundary source-sinks, no wind, 20% bathymetry, and lateral friction. Transports in 5 x 10^6 m^3/sec.

extending each case to 1800 time steps (900 days) in order to observe the long-term effects of the two driving forces. In all cases, circulation patterns remained qualitatively the same, once the steady state conditions were met. The following section will discuss the results of the next series of runs. These were conducted with the climatological wind data, as discussed earlier, applying the stress to the surface along with the source-sink driving function. Comparison runs were made with and without non-linearities and bottom friction.

IV. ACTUAL WIND DATA RESULTS

This series consisted of nine runs. They were conducted to investigate the contrast between a July and a January wind field driving force and the effects of varying bottom friction and non-linearities. Sources and sinks were added during the series for further comparisons.

The first test was conducted with two runs. Both runs used July climatological wind data as the sole driving function. Non-linearities and bottom friction were allowed to remain zero. The coriolis parameter in all cases varied with latitude as in all previous cases. The first run was a flat bottom case and the second run was with 20% bathymetry. In the first run, there was an intensified flow noticeable in the northwest corner of the area, as in the exploratory runs. This indicated that wind was forcing a westward intensification which was to be expected with the predominant prevailing southwesterly winds over the basin. The wind field had an anticyclonic perturbation in the southwestern corner. This introduced some perturbations in the flow field and even produced a negative gyre in the southwestern corner (Figure 10). After 600 time-steps, this case had reached an approximately steady state.

The second run reached steady state conditions around 420 time-steps (210 days). With the bathymetric features applied in this case, it was evident that the flow was

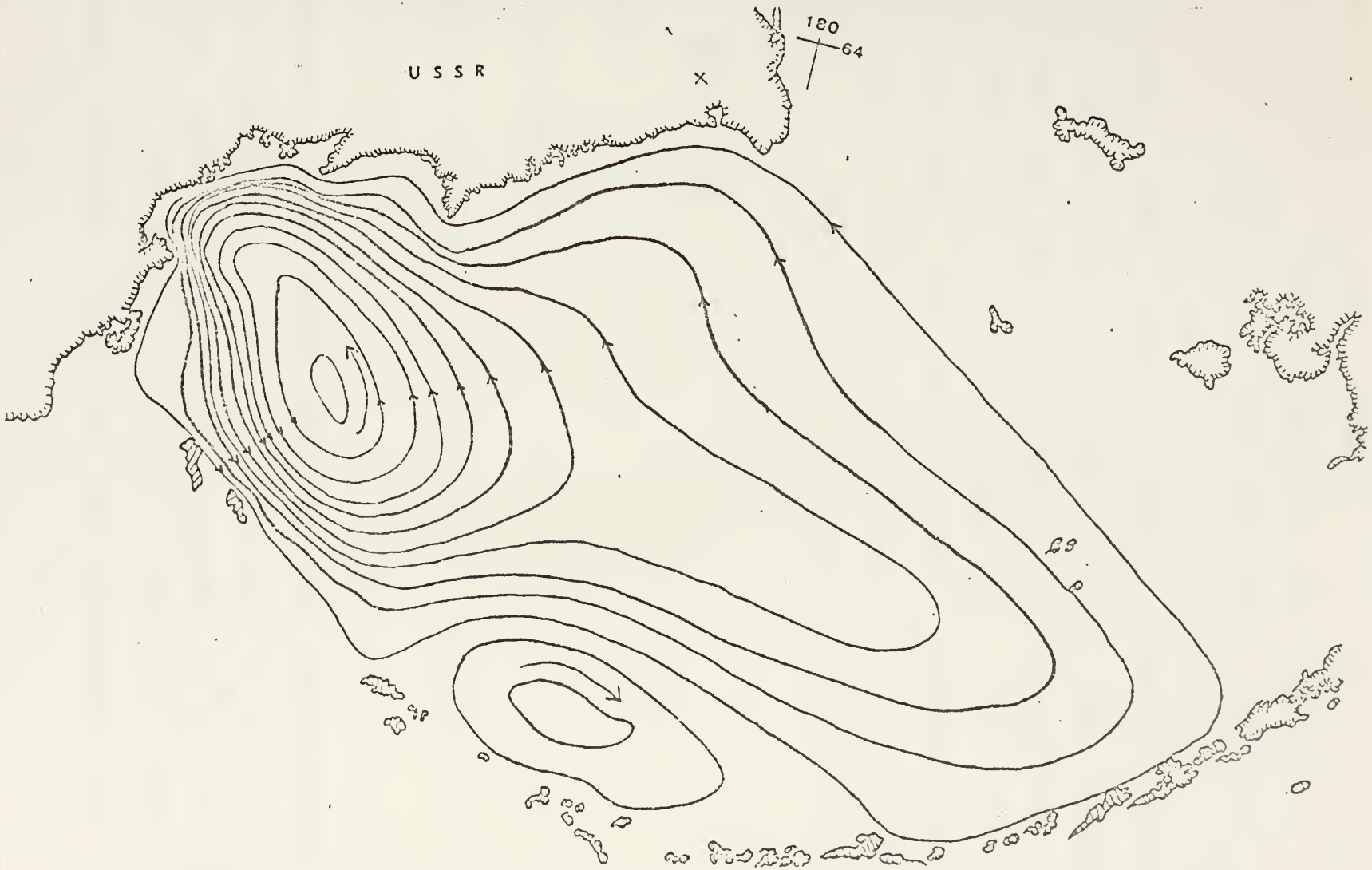

Figure 10. July wind, no source-sink, flat bottom, and lateral friction. Transports in 0.5×10^6 m^3/sec.

bathymetry-dependent (Figure 11). The gyre noticed in the first case moved around somewhat to align itself with the depth contours. Another anticyclonic gyre appeared to the east on the other side of the Bowers Ridge. The general flow pattern is cyclonic with perturbations throughout, evidently from the bathymetric effects. Transport values are reduced by one-fifth from the first case. There was some indication of cross ridge flow over the Shirshov and Bowers Ridges.

The next set consisted of three runs. These all utilized only July wind field data and excluded non-linearities. The purpose of these runs was to experiment with different values of bottom friction. Including bottom friction in the equations requires an equation of the form:

$$\frac{\partial \xi}{\partial t} = -\gamma \xi \tag{11}$$

where:

$$\gamma = \frac{k}{h}$$

This, in turn, requires an exponential solution of the form:

$$\xi = \xi_0 e^{-\frac{k}{h}t} \tag{12}$$

which is a time dependent function. This coefficient can then physically be related to a 1/e decay in the vorticity field. Therefore values were determined for $\frac{k}{h} = 1$ or $k = \frac{h}{t}$, where $k = C3 = \frac{R}{DF}$ and h was taken as the minimum depth of the model, 30 meters. Three cases were investigated where t was equivalent to 5, 10, and 20 days. These corresponded to a

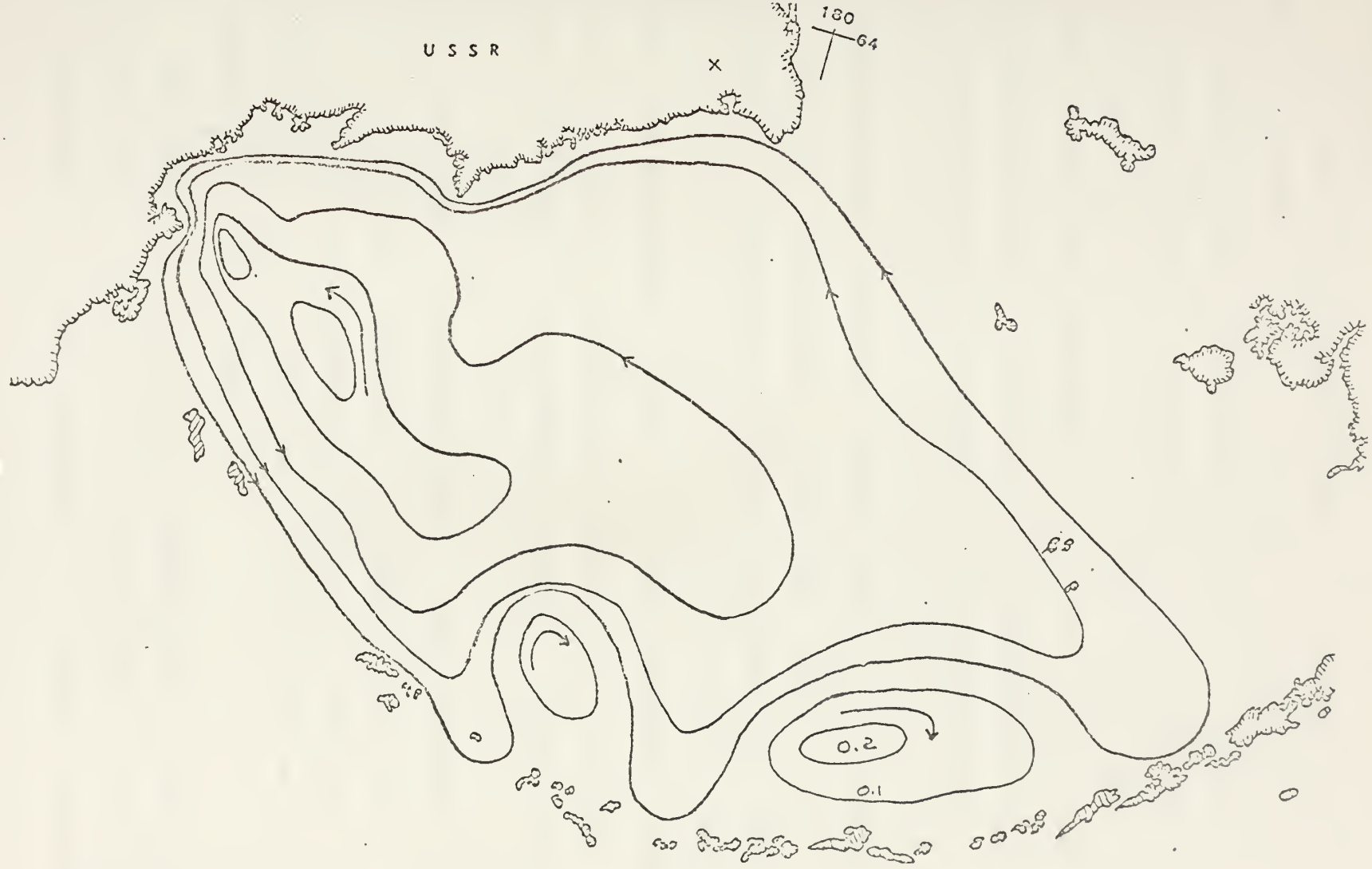

Figure 11. July wind, no source-sinks, 20% bathymetry, lateral friction. Transports in 10^6 m^3/sec.

decay time within the model of 10, 20, and 40 time steps respectively.

All three cases reached steady state conditions between 300 and 350 time steps (150-175 days). In all cases the flow patterns were very similar indicating, as expected, that the bottom friction, once applied does not quantitatively alter the flow as it is varied. In this set the flow did tend to follow the topographic relief more closely than observed previously. The value of C3 corresponding to a 10 day period was finally chosen as the representative bottom friction parameter because the implied time scale seemed reasonable under the imposed conditions (Figure 12).

The next set consisted of two runs. This set was conducted to investigate the effects of sources and sinks. The basic data used on each of the runs was the July wind field, 20% bathymetry, C3 for 10 days as determined in the last set, coriolis parameter varying with latitude and source-sink data for the western boundary. Initial conditions for this series were taken from a previous series run with only source-sink data for 900 days in order to exclude the source-sink driven transients as a complicating factor. The first run was completed excluding non-linearities (Figure 13). In the second run, non-linearities were included $\left(C1 = \frac{\psi_o}{\Delta^2 DF}\right)$ (Figure 14).

The resulting flow patterns showed gyres in the localized area where the source-sink cross-boundary transports were applied, as was to be expected. An intense pattern was

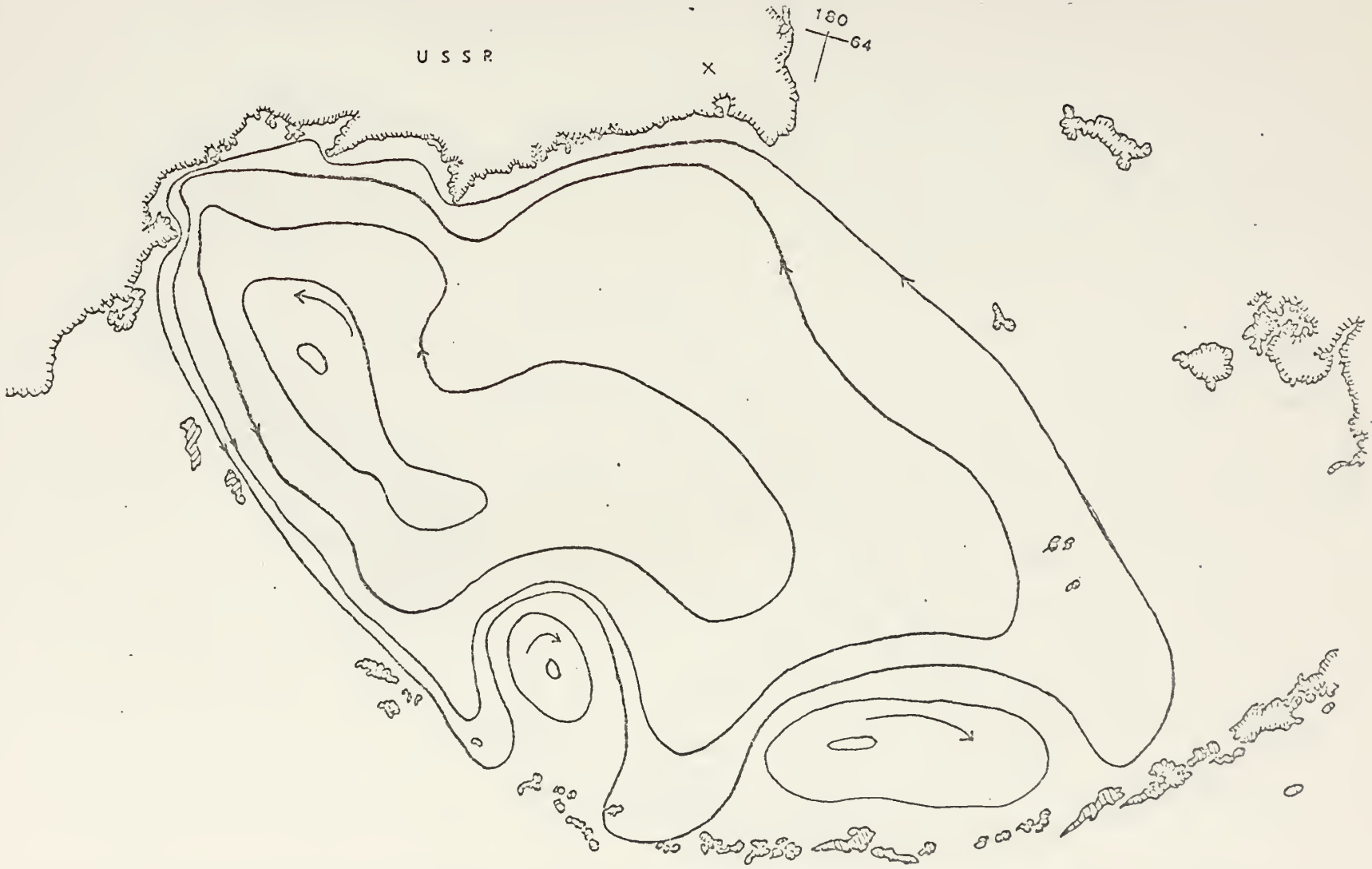

Figure 12. July wind, no source-sinks, 20% bathymetry, bottom and lateral friction. Transports in 10^6 m^3/sec.

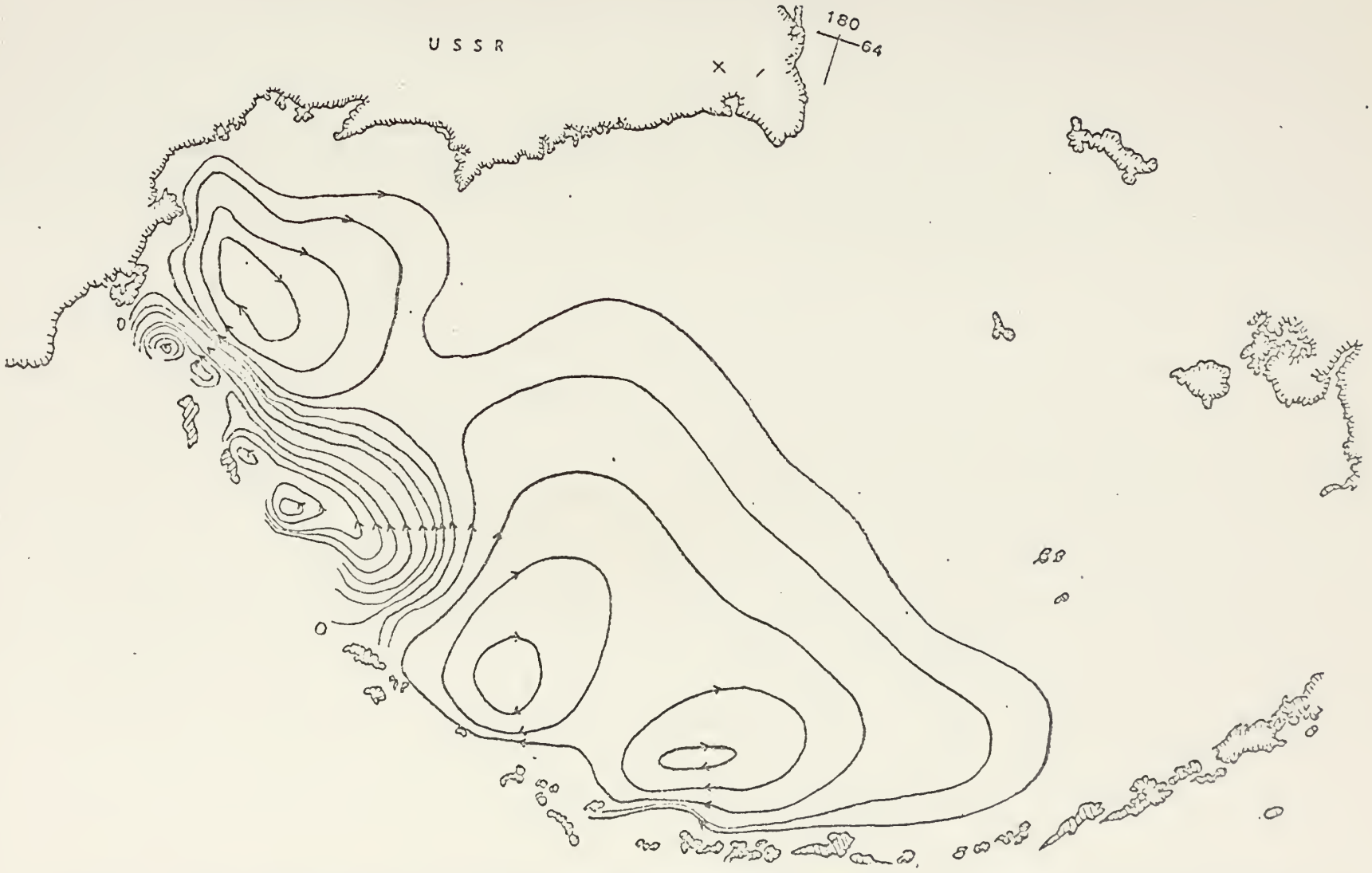

Figure 13. July wind, western boundary source-sinks, 20% bathymetry, bottom and lateral friction. Cyclonic transports: 20, 15, 10, 8, 6, 4, 2, 1; anticyclonic: 4, 3, 2, 1, 0.5; 10^6 m^3/sec.

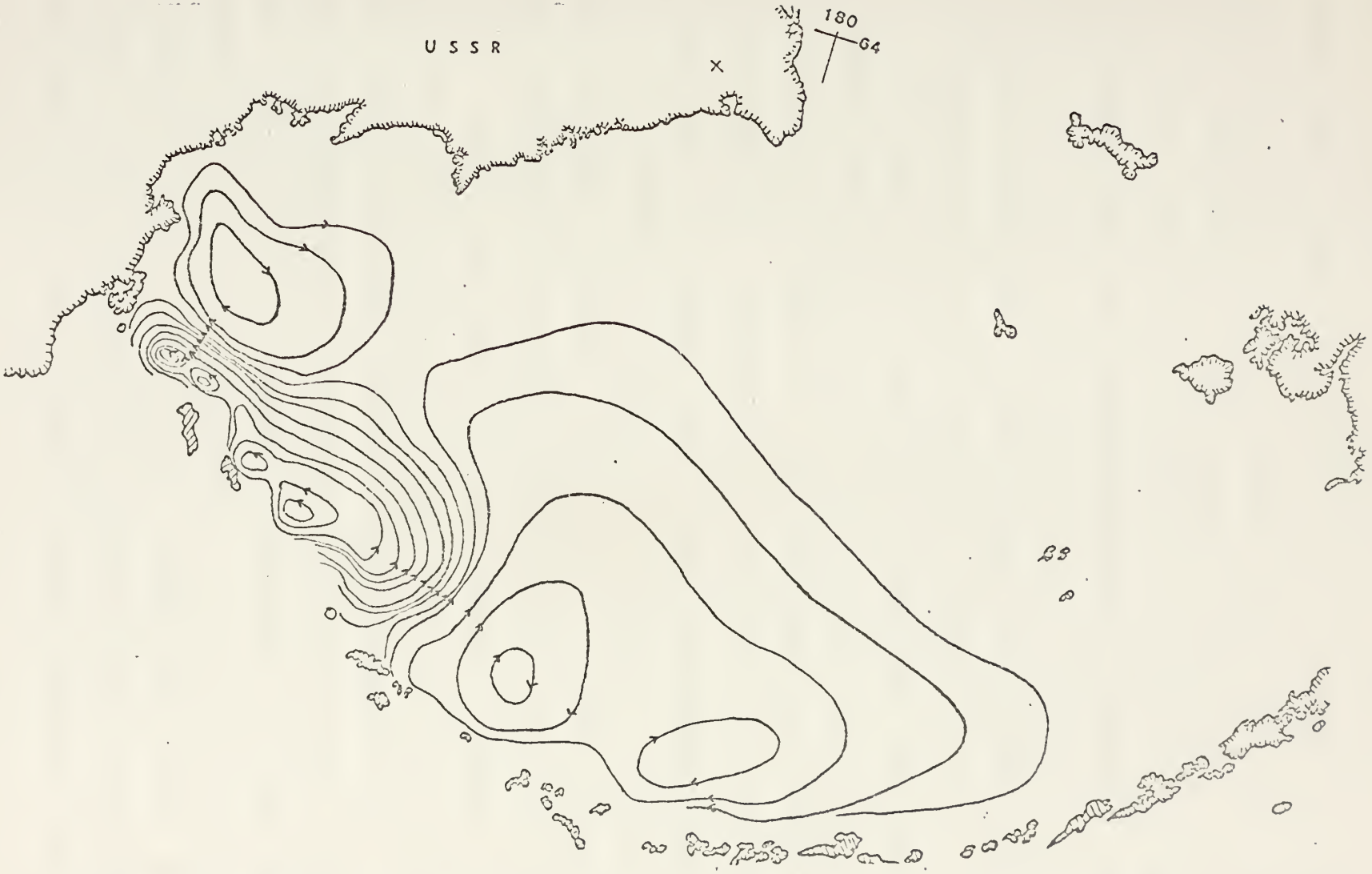

Figure 14. July wind, western boundary source-sinks, 20% bathymetry, bottom and lateral friction, and non-linearities. Transports same as in Figure 13.

set up at the interface between the motions due principally to the sources and sinks and those due to the winds. In both cases, a significant fact is that it appeared that the sources and sinks were the dominant forces in the flow field. After consideration of the relative driving forces, this was not totally unexpected. A negative gyre appeared northwest of Shirshov Ridge and the gyres previously observed on either side of the Bowers Ridge remained. Cross ridge flow was evident in both cases. In the second case, as was anticipated, the addition of the non-linearities smoothed the flow somewhat.

The last set also consisted of two runs. This time the January wind field was used. The first run was without non-linearities (Figure 15), and the second run included them (Figure 16). Smoothing was evident in the second run. January has the strongest wind field of the existing data and as such it developed stronger gyres throughout the basin area than the July wind. In this set, it became evident that the stronger wind field was influencing somewhat the force of the sources and sinks. The gyres along the western boundary were still present, as was expected in the local area of the sources and sinks, but the strong anticyclonic gyre over the remainder of the Bering Sea basin had been reduced and along the eastern portion, in particular, had even been replaced by a cyclonic perturbation. This perturbation was viewed as a direct result of the stronger wind field. In Figure 16, the non-linearities appeared to have reduced the magnitude of the gyres along the Aleutian chain and had

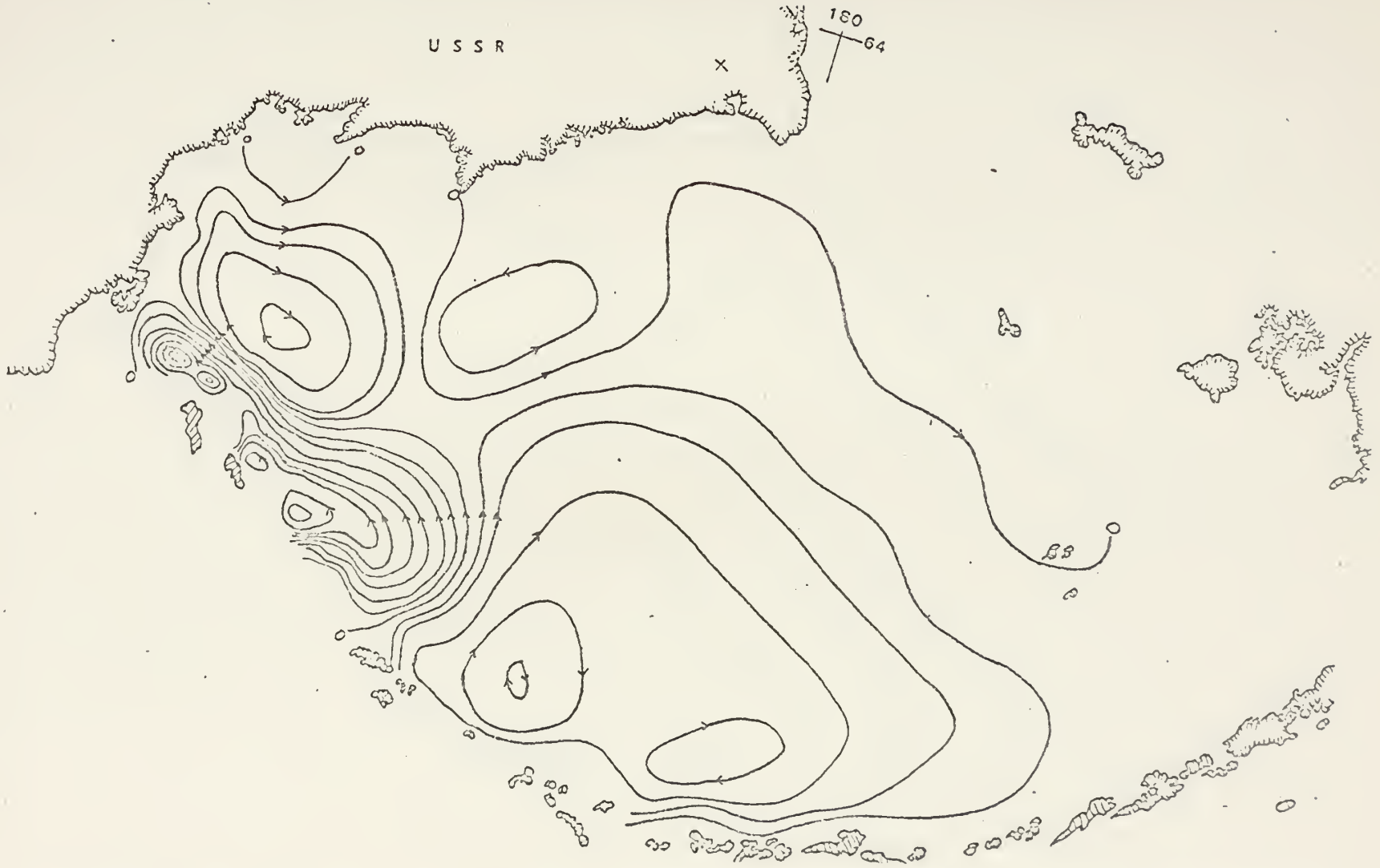

Figure 15. January wind, western Boundary source-sinks, 20% bathymetry, bottom and lateral friction. Transports same as in Figure 13.

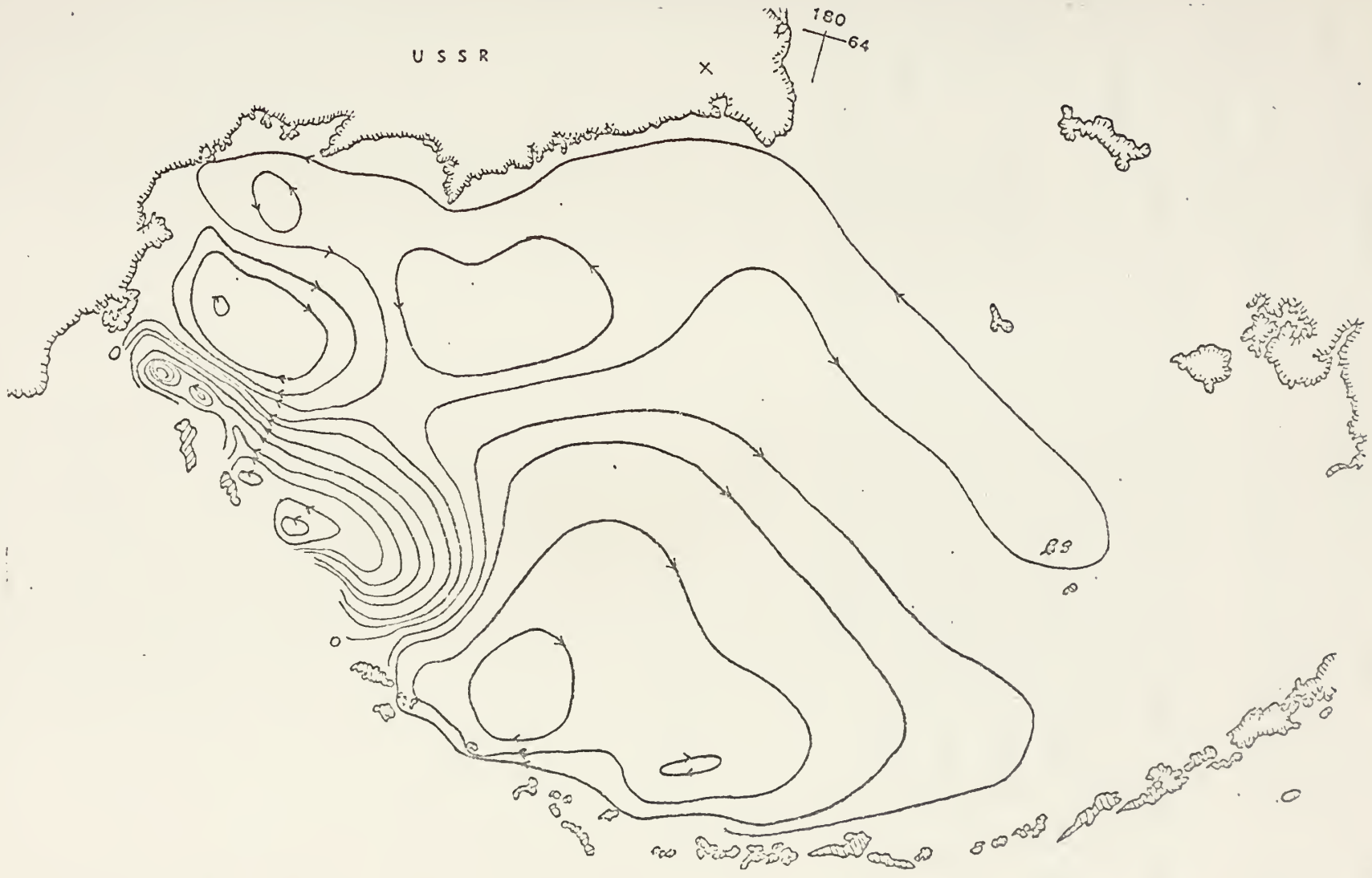

Figure 16. January wind, western boundary source-sinks, 20% bathymetry, bottom and lateral friction, and non-linearities. Transports same as in Figure 13.

definitely smoothed out the perturbation field as a result of the interaction of the true driving forces. This became noticeable along the eastern side of the basin where there now existed a possibility of a counter current due to the smoothing effect.

The counter current hinted at has also been discussed by Coachman (1973) as a possibility during certain times of the year. It is not clear that the counter current in the model is dynamically similar to the one he described. However, in order to look at this possibility more closely, the next section investigated the results of adding free slip conditions along the eastern boundary.

V. INVESTIGATION OF FREE SLIP BOUNDARY CONDITIONS

The model had been run with only no-slip conditions imposed on all boundaries at this stage. This next series was conducted to investigate the results of adding free slip conditions along the open boundary on the eastern edge of the model. This area, in the the Bering Sea, is all open water along the continental shelf and, for the most part, the depth of water is less than 300 meters.

Two separate runs were made, one with and one without bottom friction. The January wind field data was used along with the sources and sinks as the driving force. The run without bottom friction (C3 = 0), Figure 17, showed a close resemblance to Figure 16 everywhere except in the area of direct interest. Along the eastern and northern edges of the model, a definite cyclonic gyre was forming. It was confined to the continental shelf region and the Shirshov Ridge area only. The counter current possibility still existed along the continental slope and shelf areas, primarily in water less than 1000 meters deep.

In the second run, when bottom friction was added in, The cyclonic gyre spread out more in the northern sector and was forced into the western area by the Shirshov and Bowers Ridges. Along the eastern edge, there appeared to be an attempt for the counter current to follow the

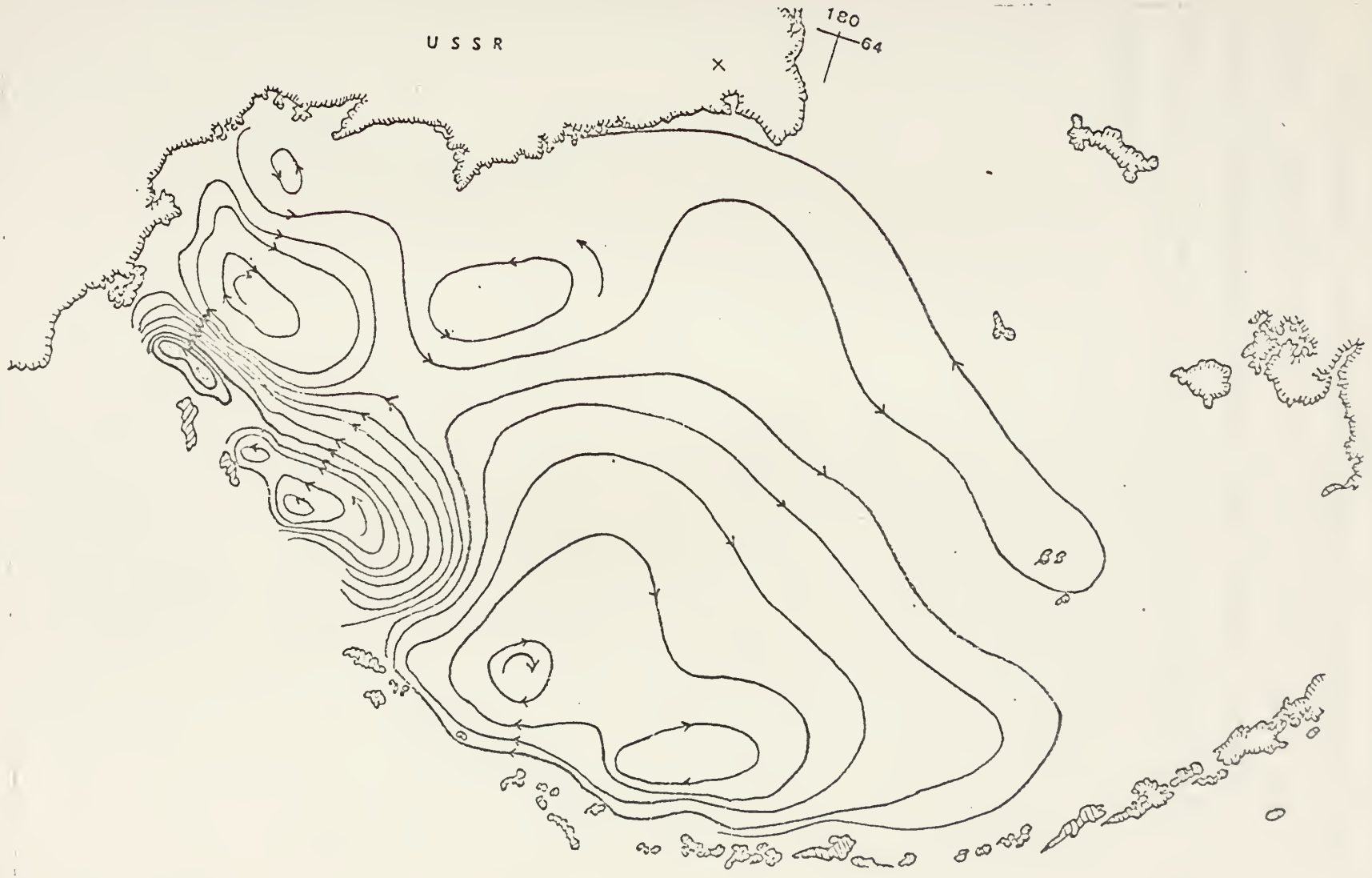

Figure 17. January wind, western boundary source-sinks, 20% bathymetry, bottom and lateral friction, and free slip. Transports same as in Figure 13.

topographic relief along the 1000 meter contour. This placed it right along the continental slope (Figure 18).

Both these runs had non-linearities included in the problem. The addition of free slip conditions along the eastern open boundary did not seem to make any appreciable difference in the flow pattern or in the magnitude of the transports.

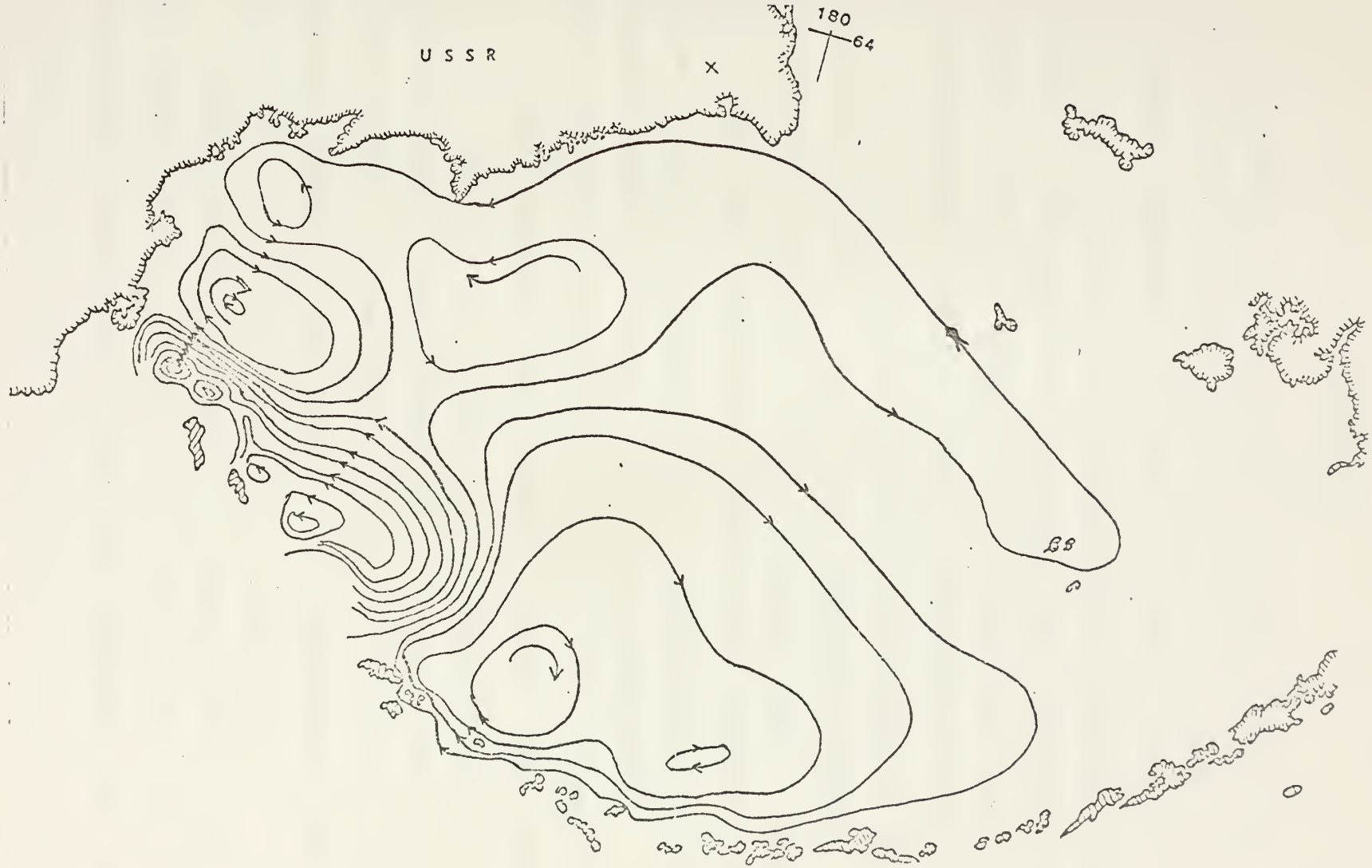

Figure 18. January wind, western boundary cource sinks, 20% bathymetry, bottom and lateral friction, non-linearities, and free slip conditions. Transports same as in Figure 13.

VI. CONCLUSIONS

Following the setting up of the model, testing for sensitivity and stability were conducted to ensure the model was working properly. To do this, an initial run under flat bottom conditions, with a constant wind force applied, was made. The results were not unexpected. The flow was cyclonic and had an obvious intensification along the western boundary similar to Munk's closed basin studies.

Actual wind data was used to drive the model in the last series of runs. This was data compiled by month. July data was the weakest field and January was the strongest. These were combined with source-sink transport exchange values along the western boundary. Comparisons were made between results of the July and January wind fields, while including and excluding bottom friction and non-linearities.

In all cases when the bathymetric factors were added, the flow became very dependent on the topographic relief. The Shirshov and Bowers Ridges tend to divide the area into three basins, the Kamchatka Basin, the Aleutian Basin, and an area between the two ridges. The overall circulation pattern was divided into gyres, one in each basin.

Initially, when looking at the wind and sources and sinks as separate driving forces, it appeared that the wind was the primary driving force. This also agreed with the results from previous researchers. The results of the Sorce-sink

driving forces alone was two principal cyclonic gyres along the western boundary and one large anticyclonic gyre over the remainder of the basin. The wind force produced a large cyclonic gyre over the entire basin. Once the two driving forces were put together, the apparent dominant force became the sources and sinks.

In the case where the wind and sources and sinks were used to drive the model, the flow became generally anti-cyclonic. There were two rather separate patterns, however. Along the western boundary the flow was definitely driven by the source-sink input. As the flow got further from the western boundary, there was an area of intensification which was a result of the interaction of the wind influence and that of the sources and sinks. Beyond that, came the major gyre that covered the remainder of the deep sea basin area. This was an anticyclonic gyre with some perturbations in the field. These were viewed as being influenced by the wind field.

July wind data was used at first and this resulted in the pattern just described. These runs had bottom friction in the equations. The effects caused by the bathymetry were much larger than the effects observed by the bottom friction. Some of the runs had non-linearities included. These showed primarily a smoothing of the flow pattern. When the January wind field data was used, the flow in the eastern portion of the area started to show the effects of the strong wind field overriding the influence of the sources and sinks.

The final set of runs were conducted to explore the differences between free slip and no slip conditions along the eastern boundary. With the stronger January wind applied in the model, the cyclonic gyre that appeared in the eastern portion also introduced the possibility of a counter current along the continental slope. By changing the initial conditions to allow free slip in that area, the counter current tended to follow bathymetry a little closer but no more than when non-linearities were added.

Hughes' proposed circulation scheme (Figure 19) was developed for the summer months and as such, the July composite runs were used for comparison. Generally, there were areas of agreement as well as disagreement. Along the western boundary, the flow pattern agree quite well. In the northwestern corner of the Kamchatka Basin, both patterns showed an anticyclonic gyre. The two patterns disagreed in the overall flow. Hughes shows a cyclonic tendency where the model has an anticyclonic circulation; particularly, just west of the Shirshov Ridge where the model showed a large negative gyre approaching two Sverdrups in the summer and three to four Sverdrups in the winter. Evident in both instances, however, is the fact that gyres throughout the Bering Sea deep water basin are predominantly dependent upon topographic relief. Cross ridge flow is also evident in both.

These comparisons have shown that for a thorough understanding of the dynamics of the Bering Sea, study must

continue along both these lines. More direct measurements are necessary, particularly along the eastern boundary at the edge of the continental slope. These would aid in probing the counter current suspected in that area. In the numerical modeling, studies are presently continuing on a time-dependent wind driven model. This study uses twelve months of climatological data. Further studies should be conducted with investigation into source-sink data along the other boundaries of the model.

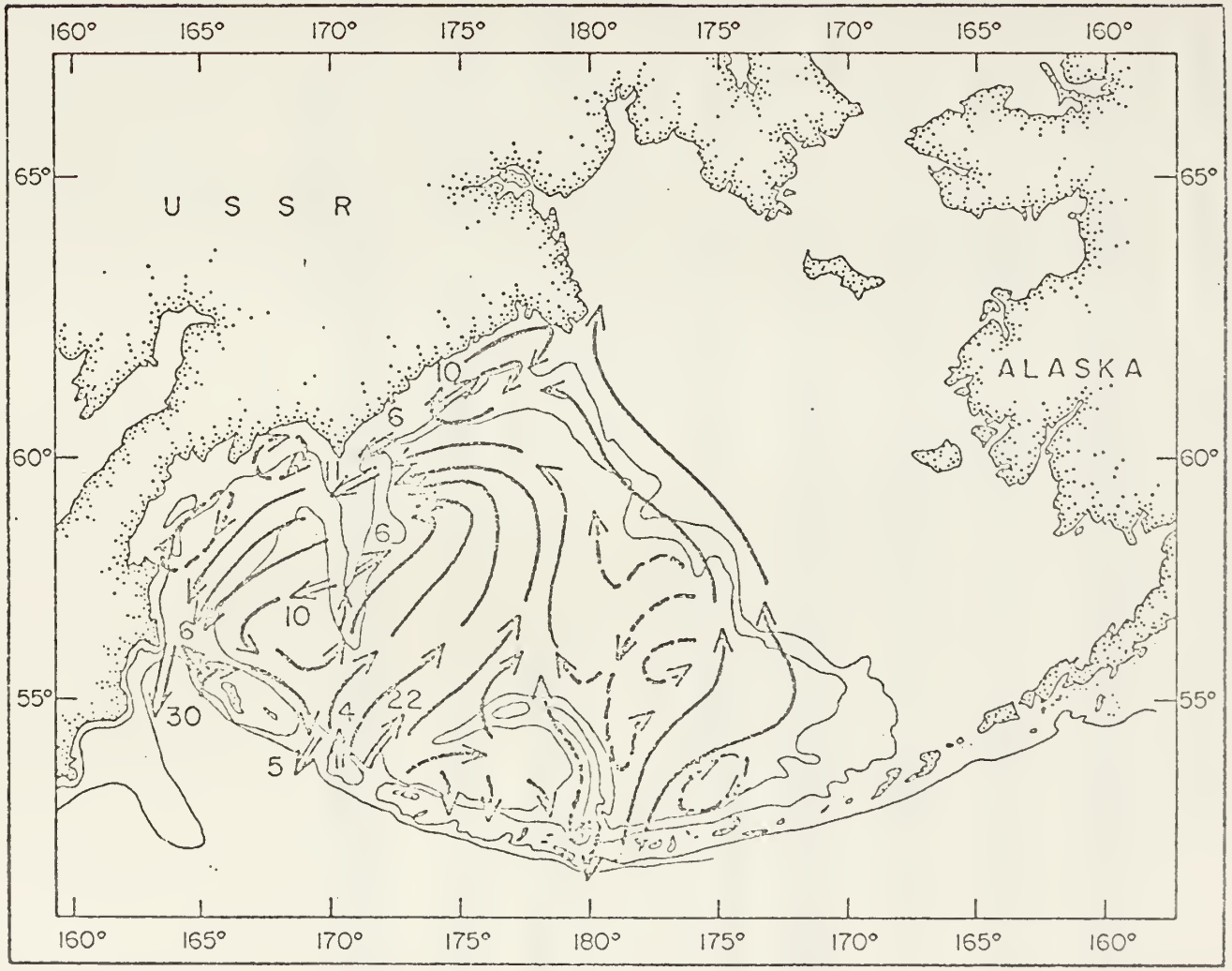

Figure 19. Proposed summer circulation scheme by Hughes (1972).

BIBLIOGRAPHY

Aagaard, Knut (1973), personal communication.

Coachman, Lawrence K. (1973), personal communication.

Naval Postgraduate School Technical Report Number NPS-58G172071A, The Development of a Homogeneous Numerical Ocean Model for the Ocean, by J.A. Galt, July 1972.

Galt, J.A., "Numerical Simulation of Arctic Ocean Dynamics," Summer Computer Simulation Conference, v. II, p. 948-952, 1972.

Galt, J.A., "A Numerical Investigation of Arctic Ocean Dynamics," Journal of Physical Oceanography, in print, October 1973.

Hughes, F.W., Circulation and Transport in the Western Bering Sea, Ph. D. Dissertation, University of Washington, Seattle, 1972.

Munk, W.H., In Robinson, A.R. (ed.), Wind Driven Ocean Circulation, Blaisdell Publishing Company, 1963, p. 25-68.

Sverdrup, H.U., Johnson, M.W., and Fleming, R.H., The Oceans, p. 732, Prentice-Hall, Inc., 1942.

Sverdrup, H.U., In Robinson, A.R. (ed.), Wind Driven Ocean Circulation, Blaisdell Publishing Company, 1963, p. 3-10.

Veronis, George, "Rossby Waves with Bottom Topography," Journal of Marine Research, v. 24, p. 388-394, 1966.

Willems, R.C., Stability and Convergence Studies on a Numerical Model of the Arctic Ocean, M. S. Thesis, Naval Postgraduate School, Monterey, California, 1972.

INITIAL DISTRIBUTION LIST

		No. Copies
1.	Defense Documentation Center Cameron Station Alexandria, Virginia 22314	2
2.	Library, Code 0212 Naval Postgraduate School Monterey, California 93940	2
3.	COMDT (GOMS 1/74) U. S. Coast Guard Washington, D.C. 20590	1
4.	Commanding Officer U. S. Coast Guard R. & D. Center Avery Point Groton, Connecticut 06340	1
5.	U. S. Coast Guard Oceanographic Unit Bldg. 159E, Washington Navy Yard Annex Washington, D.C. 20390	1
6.	Dr. J. A. Galt Department of Oceanography Naval Postgraduate School Montery, California 93940	3
7.	Lcdr. Jerry C. Bacon U.S.C.G. R. & D. Center Avery Point Groton, Connecticut 06340	3
8.	COMDT (GPTP 1/72) U.S. Coast Guard Washington, D.C. 20591	2
9.	Department of Oceanography, Code 58 Naval Postgraduate School Montery, California 93940	3
10.	Office of Naval Research, Code 480 Arlington, Virginia 22217	1

11. Oceanographer of the Navy — 1
Hoffman Building #2
2461 Eisenhower Avenue
Alexandria, Virginia 22314

12. Dr. Robert E. Stevenson — 1
Scientific Liaison Office
Scripps Institution of Oceanography
La Jolla, California 92037

13. AIDJEX — 1
Division of Marine Research
University of Washington
Seattle, Washington 98105

14. Professor Lawrence K. Coachman — 1
Department of Oceanography
University of Washington, WB-10
Seattle, Washington 98105

15. Mr. R. McGreagor — 2
Director of Arctic Section
Office of Naval Research, Code 415
Arlington, Virginia 22217

SECURITY CLASSIFICATION OF THIS PAGE (When Data Entered)

REPORT DOCUMENTATION PAGE		READ INSTRUCTIONS BEFORE COMPLETING FORM
1. REPORT NUMBER	2. GOVT ACCESSION NO.	3. RECIPIENT'S CATALOG NUMBER
4. TITLE (and Subtitle) Numerical Investigation of Bering Sea Dynamics		5. TYPE OF REPORT & PERIOD COVERED Master's Thesis; September 1973 6. PERFORMING ORG. REPORT NUMBER
7. AUTHOR(s) Jerry Craig Bacon		8. CONTRACT OR GRANT NUMBER(s)
9. PERFORMING ORGANIZATION NAME AND ADDRESS Naval Postgraduate School Monterey, California 93940		10. PROGRAM ELEMENT, PROJECT, TASK AREA & WORK UNIT NUMBERS
11. CONTROLLING OFFICE NAME AND ADDRESS Naval Postgraduate School Monterey, California 93940		12. REPORT DATE September 1973 13. NUMBER OF PAGES 62
14. MONITORING AGENCY NAME & ADDRESS(if different from Controlling Office) Naval Postgraduate School Monterey, California 93940		15. SECURITY CLASS. (of this report) Unclassified 15a. DECLASSIFICATION/DOWNGRADING SCHEDULE

16. DISTRIBUTION STATEMENT (of this Report)
Approved for public release; distribution unlimited.

17. DISTRIBUTION STATEMENT (of the abstract entered in Block 20, if different from Report)

18. SUPPLEMENTARY NOTES
This work was done in conjunction with a project under the overall guidance of Dr. J.A. Galt, sponsored by the Arctic Section of the Office of Naval Research.

19. KEY WORDS (Continue on reverse side if necessary and identify by block number)
Bering Sea
Numerical Model
Surface Circulation
Ocean Dynamics

20. ABSTRACT (Continue on reverse side if necessary and identify by block number)
Galt's (1972) Arctic numerical model was used to explore the significant dynamics of the Bering Sea. The model was set up and tested for numerical stability. Climatological wind fields were used along with source-sink exchange transports to drive the model. The runs investigated the results of adding or deleting bottom friction, non-linearities and bathymetry. The results obtained by the model were compared to a circulation pattern proposed by Hughes (1972). The model showed that the circulation is strongly bathymetry-dependent and primarily driven by the sources and sinks.

DD FORM 1 JAN 73 1473 EDITION OF 1 NOV 65 IS OBSOLETE
S/N 0102-014-6601 |
(Page 1)

SECURITY CLASSIFICATION OF THIS PAGE (When Data Entered)